



Contents lists available at ScienceDirect

Chinese Chemical Letters

journal homepage: www.elsevier.com/locate/ccllet

Biochar with self-doped N to activate peroxymonosulfate for bisphenol-A degradation *via* electron transfer mechanism: The active edge graphitic N site

Yun-Xin Huang^{a,1}, Lin-Qian Yu^{a,1}, Ke-Yu Chen^a, Hao Wang^a, Shou-Yan Zhao^a,
 Bao-Cheng Huang^{a,b,*}, Ren-Cun Jin^a

^a School of Engineering, Hangzhou Normal University, Hangzhou 311121, China

^b Zhejiang Provincial Key Laboratory of Urban Wetlands and Regional Change, Hangzhou 311121, China

ARTICLE INFO

Article history:

Received 25 September 2023

Revised 22 November 2023

Accepted 13 December 2023

Available online 22 December 2023

Keywords:

Peroxymonosulfate

Carbon-based catalysts

Edge graphitic-N

Non-radicals

Bisphenol A

ABSTRACT

Environmental endocrine disruptors, represented by bisphenol A (BPA), have been widely detected in the environment, bringing potential health risks to human beings. Nitrogen-containing biocarbon catalyst can activate peroxymonosulfate (PMS) to degrade BPA in water, but its active sites remain opaque. Herein, in this work, nitrogen-containing biochar, *i.e.*, C-N_{edge}, enriched with graphitic-N defects at the edges was prepared by one-pot co-pyrolysis of chitosan and potassium carbonate. The results showed that the C-N_{edge}/PMS system can effectively degrade 98% of BPA (50 mg/L). The electron transfer based non-radical oxidation mechanism was responsible for BPA degradation. Edge graphitic-N doping endows biochar with strong electron transfer ability. The catalyst had good recovery and reuse performance. This catalytic oxidation was also feasible for other refractory pollutants removal and worked well for treating practical wastewater. This work may provide valuable information in unraveling the N doping configuration-activity relationship during activating PMS by biochar.

© 2024 Published by Elsevier B.V. on behalf of Chinese Chemical Society and Institute of Materia Medica, Chinese Academy of Medical Sciences.

With the ever-increased desire on designing environmental benign material for wastewater remediation, carbon-based catalysts are gaining extensive attentions by researchers [1,2]. Carbon materials own peculiarities of large specific surface area, abundant reserves, and acid/alkali resistance, which endows its great potential for practical application. Advanced oxidation process is widely used to degrade and mineralize organic pollutants due to its ability to produce highly reactive substances. The choice of oxidant is crucial in advanced oxidation process, which includes peroxymonosulfate (PMS), peroxydisulfate, hydrogen peroxide as well as peracetic acid [3,4]. In the past years, carbon materials were found efficaciously in PMS activation [5–7]. However, the degree of graphitization [8], type of oxygen-containing functional groups on the surface [9], porosity [10], and metal or mineral impurities [11] all take effect on catalytic activity. Therefore, it is of extraordinary significance to improve the PMS activation efficiency of non-nano carbon materials and elucidate their active centers.

Through theoretical simulation and experimental verification, nitrogen doping can regulate the electronic structure of the six membered carbon ring of carbon material, promoting the electron-transfer ability [12] and enhancing catalytic activity of carbon materials. The doped nitrogen can actually assume different configurations, including pyridinic N, pyrrolic N, and graphitic N [13]. Due to the diversity and variability of different nitrogen configurations in the persulfate activation system, extensive studies are still needed to reveal the N doping configuration-activity relation in biochar based catalytic materials.

Based on the available literature reports, it is known that graphitic N had two different positional isoforms, namely graphitic center N located in the plane and graphitic edge N located at the edge [14]. The graphitic N in the planar center was considered to be the intrinsic active site for O–O bond cleavage to produce ¹O₂ in PMS, which was responsible for organic matter degradation [15]. In another study, it was revealed that the gradual removal of the carbon edge unstable N configuration under high-temperature pyrolysis induced a conformational transition from graphitic-centered N to graphitic-edge N sites [14]. The edge graphitic N can also be imaginatively referred to as “fjord edge N” [16], and this spatial effect has a great impact on material catalytic activity. Herein, we

* Corresponding author at: School of Engineering, Hangzhou Normal University, Hangzhou 311121, China.

E-mail address: huangbc@hznu.edu.cn (B.-C. Huang).

¹ These authors contributed equally to this work.

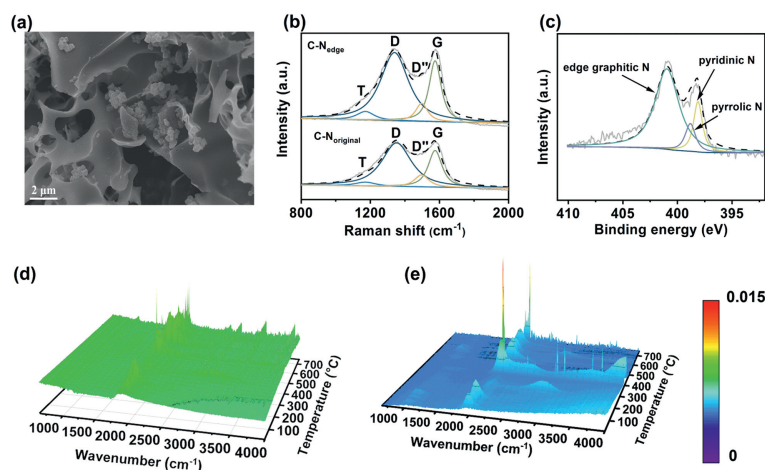


Fig. 1. Catalyst structure property characterization. (a) The SEM image of C-N_{edge}; (b) Raman spectra of the catalysts; (c) N 1s XPS spectrum of C-N_{edge}; TG-FTIR spectrum changes during pyrolysis of (d) chitosan and (e) chitosan plus K₂CO₃.

might be able to construct an electron transfer regime dominated non-radical oxidation system for refractory pollutants removal via modulating the N doping configuration of biochar.

The inspiration of this work came from the fact that the carbon and nitrogen in the biomass such as chitosan will partially volatilize under the help of pore-forming agent potassium carbonate and condition of high carbonization temperature (700–800 °C) [17], which may benefit edge graphitic N formation on the catalyst. Based on this, we prepared nitrogen-containing biochar enriched with nitrogen defects in marginal graphite, *i.e.*, C-N_{edge}, to degrade the representative refractory pollutant - bisphenol A (BPA) via activating PMS. Experiments were performed to evaluate its catalytic activation and to identify the main active substances present in its system. At the same time, we also verified the potential applications of C-N_{edge}. This work may provide valuable information in unraveling the relation between the N doping configuration and catalytic activity.

Initially, the impact of preparation parameters, *i.e.*, potassium carbonate amount and pyrolysis temperature, on catalyst activity was evaluated (Fig. S1 in Supporting information). The catalyst (C-N_{edge}) prepared at a chitosan and K₂CO₃ ratio of 3:5 and a carbonization temperature of 750 °C was selected for the following studies to investigate the correlation between the nitrogen-doped configuration and the catalytic activity. To understand the microstructure of the catalyst, the morphology of C-N_{original} and C-N_{edge} were preliminarily characterized by SEM. The SEM images showed that C-N_{original} was block-like and without obvious pore structure (Fig. S2 in Supporting information). After adding K₂CO₃, the surface of C-N_{edge} formed a pore structure (Fig. 1a), which indicated that C-N_{edge} might own a larger specific surface area. The N₂ adsorption-desorption isotherms and pore size analysis (Figs. S3a and b in Supporting information) further showed that the co-pyrolysis with K₂CO₃ favored the formation of pores, and the ratio of micropores and mesopores was higher in C-N_{edge} compared to C-N_{original}, reaching 90%, and the specific surface area of C-N_{edge} was up to 2328.4 m²/g (Table S1 in Supporting information). The specific surface area test of the catalyst is consistent with that of the SEM images.

The Raman shift of catalysts showed the content of graphitic and defective-C structures in the catalyst. Two carbon-related characteristic peaks located at 1340 cm⁻¹ (D-band) and 1590 cm⁻¹ (G-band) could be observed from Raman spectra (Fig. 1b), which respectively represented the sp² hybrid carbon (defective carbon) and sp³ hybrid carbon (graphitic carbon) [18]. The I_D/I_G values can reflect the defect degree of the catalyst [19]. The estimated I_D/I_G

value of C-N_{original} was 2.30 and that of C-N_{edge} was 2.61, which clearly implied that co-pyrolysis of chitosan and potassium carbonate would increase the defect degree of the obtained product. Due to the reduction of N heteroatoms in the carbon skeleton, the area of the D band decreased, leading to more exposed edge structures. The increase of the T-band area confirm that these exposed edge structures can promote the generation of edge nitrogen doped configurations [20].

Pyrrolic N (400.5 eV) [21] and pyridinic N (398.6 eV) [22] were the two main peaks in the N 1s XPS of C-N_{original} (Fig. S4 in Supporting information). C-N_{edge} were mainly edge graphitic N (402.6 eV) [14], Pyrrolic N (400.5 eV) [21] and pyridinic N (398.6 eV) [22] (Fig. 1c). Combined with organic element analysis (Table S2 in Supporting information), it is considered that the nitrogen content of the two catalysts is different. The reason may be that during the carbonization process, K₂CO₃ dissociates into CO₂ and K₂O to corrode the pyrrolic N structure of the carbon material, leading to a large amount of marginal graphitic N formation.

To explore the change of chitosan during pyrolysis, the TG test was first carried out. As shown in Fig. S5 (Supporting information), C-N_{original} and C-N_{edge} had a similar weight-loss curve, where both lost weight at around 260 °C. However, at 750–800 °C, the decrease trend of C-N_{edge} was slower than that of C-N_{original}, the reason may be that K₂CO₃ was partially decomposed at higher temperatures and had less loss, which was conducive to the formation of edge graphitic N in chitosan. Secondly, combined with TG-FTIR spectra (Figs. 1d and e), obvious peaks can be observed at temperature of 400–500 °C, showing that both samples release CO₂ (2349 cm⁻¹) during calcination. However, when K₂CO₃ was added, a C≡N peak (2222–2260 cm⁻¹) appeared between 700 °C and 800 °C (Fig. 1e), implying possible N cleavage and edge graphitic N formation on C-N_{edge}.

The PMS dissociation catalyzed by C-N_{edge} and C-N_{original} was initially evaluated. As shown in Fig. 2a, C-N_{edge} could catalyze about 70% of PMS decomposition within 30 min, while C-N_{original} had almost no catalytic effect on PMS. The apparent rate constant (*k*_{obs}, min⁻¹) of PMS decomposition catalyzed by C-N_{edge} was 0.027 min⁻¹, which was 27-fold higher than that of C-N_{original} (0.001 min⁻¹) (Fig. 2b and Fig. S6 in Supporting information), indicating its superior catalytic activity. When BPA was added to the PMS solution, the concentration of PMS did not decrease (Fig. S7 in Supporting information), indicating that BPA had no effect on the dissociation of PMS. Then, the pollutant removal performance of the catalytic system was investigated by selecting BPA as a representative refractory pollutant. Since C-N_{edge} had a high specific

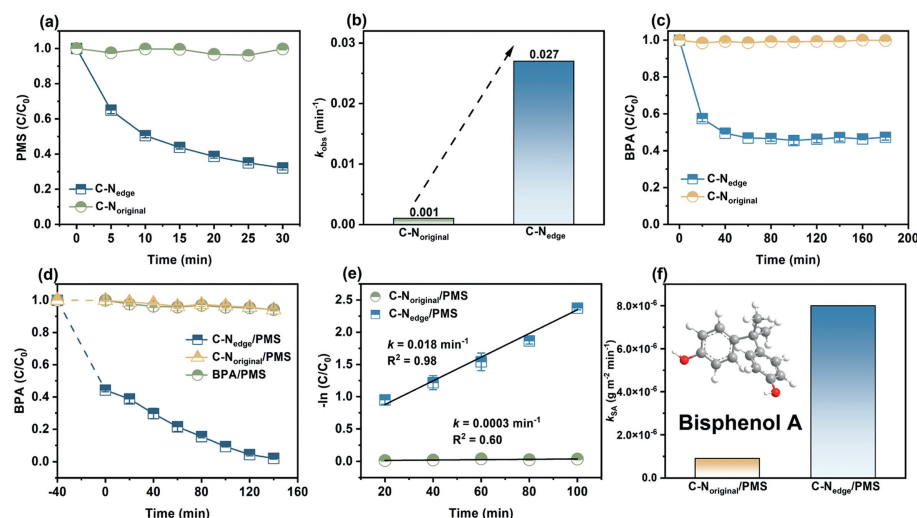


Fig. 2. Catalytic degradation performance evaluation. (a) PMS decomposition catalyzed by the C-N_{edge} and C-N_{original} and (b) the related decomposition rate constants. (c) Adsorption and (d) degradation curves of BPA by different reaction systems. (e) Pseudo-first-order kinetics fitting curve of BPA degradation. (f) Relationship between the specific activities (k_{SA}) of different catalysts. Reaction conditions: [catalysts] = 0.05 g/L, [BPA] = 50 mg/L, [PMS] = 2 mmol/L, pH 7.0.

surface area, adsorption experiments were required to determine the adsorption equilibrium time and exclude the effect of adsorption on BPA degradation. As shown in Fig. 2c, catalyst reached adsorption equilibrium after about 40 min and C-N_{edge} adsorbed about 51% of BPA. Degradation experiments (Fig. 2d) showed that both PMS and C-N_{original}/PMS systems were unable to oxidize BPA and the pH of the three reaction systems remained stable (Fig. S8 in Supporting information). After 160 min of reaction, almost all BPA was degraded in the C-N_{edge}/PMS system. The results of the degradation curve fitting indicated that the BPA removal followed *pseudo* first-order kinetics (Fig. 2e), and the reaction rate constants were calculated to be 0.018 min⁻¹ and 0.0003 min⁻¹ for C-N_{edge}/PMS and C-N_{original}/PMS, respectively. The apparent rate constants obtained from the degradation experiments were further normalized by the specific surface area of the catalysts to obtain specific rate constants (k_{SA} , g m⁻² min⁻¹) [23], to compare the catalytic activity of the two catalysts. The normalized apparent rate constant for C-N_{edge} were 8 times higher than C-N_{original} (Fig. 2f), indicating its well catalytic degradation performance. What's more, compared with the previously reported references, C-N_{edge} also had high catalytic performance (Table S3 in Supporting information).

In order to explore the mechanism of activating PMS to degrade BPA by C-N_{edge}/PMS, different quenchers were selected and added, where EtOH was used to both quench ·OH and SO₄^{·-} while TBA was for quenching ·OH [24], and L-histidine was for quenching ¹O₂ [25]. The quenching results (Fig. 3a) showed that both EtOH and TBA did not inhibit BPA degradation in the C-N_{edge}/PMS system, while L-histidine retarded the degradation rate of BPA, indicating that there may be ¹O₂ in this system. EPR spectra illustrated that the signal of DMPOX appear (Fig. S9 in Supporting information) when DMPO was added, but not the characteristic signal of 1:2:1:2:1. The appearance of the DMPOX signal may be due to the strong oxidizing nature of the C-N_{edge} surface. TEMP can specifically capture ¹O₂, producing TEMP-¹O₂ with a 1:1:1 triplet state characteristic peak [26]. As shown in Fig. 3b, a typical 1:1:1 triplet state characteristic peak was observed after mixing C-N_{edge} with PMS, demonstrating the possible production of ¹O₂. Since ¹O₂ can prolong the life in D₂O [27], the degradation of pollutants in H₂O and D₂O by C-N_{edge}/PMS system was compared, which can effectively prove the role of ¹O₂ in the reaction system. As shown in Fig. 3c, the degradation of BPA was not accelerated in D₂O, which contradicts the previous findings on ¹O₂. Although EPR

and quenching experimental results might indicate the possible ¹O₂ dominated oxidation mechanism, the recent up-to-date studies provide the opposite interpretation. First of all, it was revealed that common oxidants such as PMS and peracetic acid would directly oxidize TEMP into TEMPO, causing false positive results [28]. Secondly, the high surface area and porosity of C-N_{edge} provides abundant adsorption sites for L-histidine, which might lead to the activate sites coverage and declined catalytic activity. A similar result was also obtained in a recent study by Zhou *et al.* [29]. Consequently, we excluded the possible ¹O₂ generation in this study, while another non-radical oxidation pathway, *i.e.*, electron transfer, might exist [30,31].

We next verified the existence of electron transfer mechanism in the C-N_{edge}/PMS system, and the *in situ* infrared spectroscopy test was carried out. As shown in Fig. 3d, the infrared spectrum of PMS had an obvious vibration peak at about 1100 cm⁻¹, representing the vibration of O=S=O structure in PMS [32]. When PMS and catalyst are added together, the peak position of O=S=O in PMS had a blue shift of about 7 cm⁻¹, to the peak position of 1107 cm⁻¹. It represents that PMS was bound to the catalyst, which was one of the evidence of electron transfer in the degradation of BPA by C-N_{edge}/PMS system [33]. In addition, the constant potential time-to-current response test that had been widely adopted as an effective electrochemical method to demonstrate the presence of electron transfer [34] was conducted. As shown in Fig. 3e, adding BPA stimulated a significant increase in current output. This showed that BPA was first absorbed by C-N_{edge} catalyst, and then directly provided electrons to PMS, which is used as the electronic channel for oxidation [35]. Furthermore, we set up a galvanic oxidation reactor [36,37], so BPA can only be oxidized *via* ETP (Fig. S10 in Supporting information). After respectively adding BPA and PMS into separate two half-cells, a stable electric current could be observed. This proved that electrons can be transferred from BPA to PMS through conducting C-N_{edge}, resulting in the decomposition of PMS and the simultaneous degradation of BPA.

A good conductivity of catalyst is the prerequisites for its good electron transfer ability. Therefore, the charge transfer resistance (R_{ct}) of the catalyst was measured by electrochemical impedance spectroscopy [38], and the results were shown in Fig. 3f and Table S4 (Supporting information). Compared with C-N_{original} (R_{ct} = 27,380 Ω), C-N_{edge} (R_{ct} = 2398 Ω) had a smaller charge transfer resistance, which indicated that the addition of potassium carbonate in the carbonization process can significantly increasing

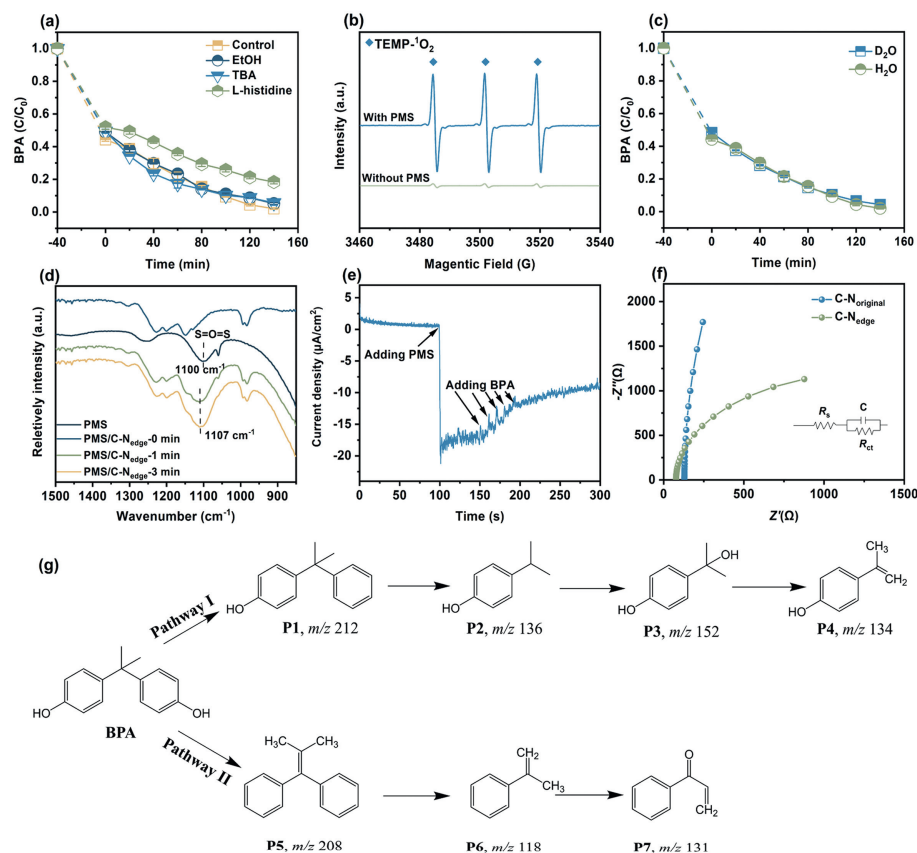


Fig. 3. Reactive oxidative species identification. (a) Effect of EtOH, TBA and L-histidine on BPA degradation in the C-N_{edge}/PMS systems. (b) TEMP-trapped ¹O₂ EPR spectra. (c) BPA degradation performance by exchanging solvent from H₂O to D₂O. (d) *In situ* FTIR spectra changes after mixing C-N_{edge} with PMS. (e) Amperometric *I-t* curve. (f) EIS of catalysts. (g) Proposed pathways of BPA degradation in C-N_{edge}/PMS system. Reaction conditions: [catalysts]=0.05 g/L, [BPA]=50 mg/L, [PMS]=2 mmol/L, pH 7.0, [EtOH]=[TBA]=200 mmol/L, [L-histidine]=20 mmol/L, [DMPO]=[TEMP]=60 mmol/L.

the conductivity of the catalyst, and the good conductivity was also the premise for the strong electron transfer ability of C-N_{edge} in the process of activating PMS to degrade BPA [39].

In order to understand the possible degradation pathways of BPA, the intermediates were analyzed by HPLC-MS/MS and seven intermediates were identified (Table S5 and Fig. S11 in Supporting information). Based on the identified intermediates and previous studies [40–44], a possible degradation pathway for BPA was proposed (Fig. 3g). Firstly, in pathway I, the C–C bond between the benzene rings was broken to form P2 [43] and direct electron transfer pathways induced the subsequent formation of P3 and P4 [41]. Next, in pathway II, the C–O bond bound to the benzene ring was cleaved, and then the hydroxyl group separated from the BPA, leading to the formation of P5 [43]. P6 and P7 may be further produced by breaking the C single bond C bond connecting the two benzene rings [40].

Catalytic stability is very important in the catalytic system [45], recycling tests were conducted to assess the stability and reusability of C-N_{edge} for the PMS-based degradation system. The result showed that the degradation rate of BPA in the C-N_{edge}/PMS system was still as high as 84% after three times of recycling (Fig. 4a). Metal center was reported to be easily deactivated and then induced the catalytic performance decline [45]. However, in this work, no metal sites were present in the C-N_{edge}. Herein, it was deduced that the decrease in the catalytic performance of the C-N_{edge} might be due to the masking of the active sites by the formed intermediates. To verify the above assumption, the C-N_{edge} after 3-cycle of use was collected and treated by ethanol rinsing or pyrolysis. Either ethanol washing or pyrolysis disposal was efficient in recovering catalytic activity of C-N_{edge} (Fig. S12 in Sup-

porting information). In order to evaluate the feasibility of applying C-N_{edge} into different water bodies treatment, this study selected tap water, Yuhangtang River water and secondary effluent of sewage treatment plant as representative water bodies to conduct BPA degradation experiments. It can be seen from Fig. 4b that the C-N_{edge}/PMS system had a high removal rate under the condition of different water body. Consistently, SEM image (Fig. S13 in Supporting information) and XRD pattern (Fig. S14 in Supporting information) of C-N_{edge} catalyst before and after degradation experiment showed negligible changes. The C-N_{edge}/PMS system not only showed good removal effect on BPA, but also had good degradation effect on other pollutants. As shown in Fig. 4c, the C-N_{edge}/PMS system can achieve rapid degradation of DCF, Triclosan and 2,4,6-TCP. Considering that the wastewater is rich in inorganic anions and natural organic matter, the effects of some inorganic anions (e.g., Cl⁻, HCO₃⁻, H₂PO₄⁻) and HA on the degradation of BPA by C-N_{edge} catalyzed PMS were evaluated (Fig. 4d). These composite substrates had no significant effect on the degradation of BPA, indicating that C-N_{edge} may be a potential environmental recovery catalyst.

In this work, biochar self-doped with edge graphitic N was successfully fabricated *via* one-pot co-pyrolysis of chitosan and potassium carbonate. Under the set test conditions, a very small amount of C-N_{edge} (0.05 g/L) can catalyze PMS decomposition to degrade 98% of BPA (50 mg/L) in 140 min. After three times of recycling, the degradation efficiency of BPA still reached 84%, indicating its good reuse ability. Multiple characterization and analytical methods verified that electron transfer mechanism was the dominated pathway for BPA degradation and the edge graphitic N with strong electron transfer ability was identified as the responsible active site. Also,

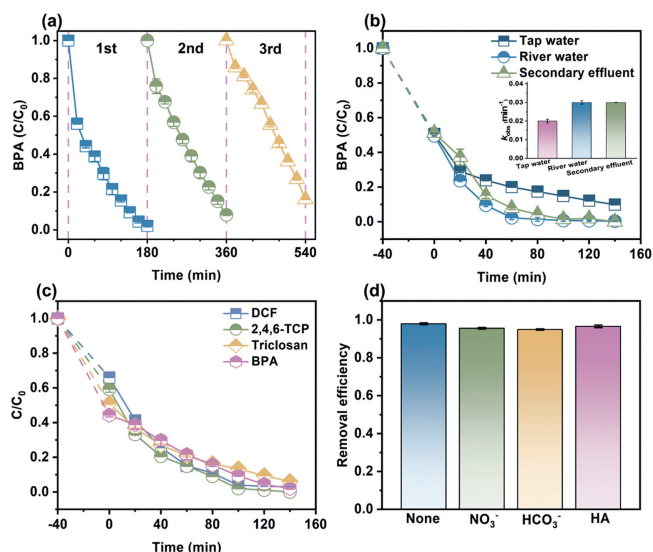


Fig. 4. Feasibility of applying the as-prepared biochar for actual wastewater remediation. (a) Recovery and reuse ability of C-N_{edge}. (b) The degradation curves of BPA in different water bodies (the inset figure is *Pseudo*-first-order kinetics). (c) Feasibility of removing other refractory organic pollutants by C-N_{edge}/PMS system. (d) Interference by background dissolved solutes. Reaction conditions: [C-N_{edge}] = 0.05 g/L, [DCF] = [2,4,6-TCP] = [Triclosan] = 50 mg/L, pH 7.0, [PMS] = 2 mmol/L, [Cl⁻] = [HCO₃⁻] = [H₂PO₄⁻] = 2 mmol/L, [HA] = 2 mg/L.

the C-N_{edge}/PMS catalytic oxidation system was efficient to other refractory pollutants removal, and was not interfered by inorganic anions in water, indicating that C-N_{edge} may be a stable and workable catalyst for remediating wastewater under environmental conditions. The results of this work are valuable for in-depth understanding the N-doping configuration on activating PMS for wastewater remediation by biochar.

Declaration of competing interest

The authors declare that they have no known competing financial interests or personal relationships that could have appeared to influence the work reported in this paper.

Acknowledgments

The authors wish to thank the National Natural Science Foundation of China (No. 51908172) and “Pioneer” and “Leading Goose” R&D Program of Zhejiang (No. 2023C03149) for the financial support of this work.

Supplementary materials

Supplementary material associated with this article can be found, in the online version, at doi:10.1016/j.ccl.2023.109437.

References

- [1] X. Zhou, C. Zhao, G. Wu, J. Chen, Y. Li, Appl. Surf. Sci. 459 (2018) 354–362.
- [2] S. Zhu, X. Li, J. Kang, X. Duan, S. Wang, Environ. Sci. Technol. 53 (2019) 307–315.
- [3] K. Hou, P. Shen, Z. Wang, et al., Chin. Chem. Lett. 34 (2023) 107555.
- [4] F. Chen, L.L. Liu, J.H. Wu, et al., Adv. Mater. 34 (2022) 2202891.
- [5] W. Xue, S. Cao, R. Liu, et al., Chemosphere 248 (2020) 126053.
- [6] S. Yang, X. Duan, J. Liu, et al., Appl. Catal. B 267 (2020) 118701.
- [7] J. Xie, X. Pan, C. Jiang, et al., Environ. Res. 236 (2023) 116745.
- [8] W. Gao, Z. Lin, H. Chen, et al., J. Anal. Appl. Pyrolysis 167 (2022) 105700.
- [9] W. Yang, Y. Liu, J. Pan, Environ. Technol. Innov. 22 (2021) 101411.
- [10] R. Hu, J. Xiao, T. Wang, et al., Chem. Eng. J. 379 (2020) 122388.
- [11] J. Zhou, X. Ren, Z. Liu, S. Yuan, Mater. Today Sustain. 20 (2022) 100225.
- [12] H.B. Qiu, P.C. Guo, L. Yuan, et al., Chin. Chem. Lett. 31 (2020) 2614–2618.
- [13] P. Matter, L. Zhang, U. Ozkan, J. Catal. 239 (2006) 83–96.
- [14] Q. Lai, H. Zheng, Z. Tang, et al., ACS Appl. Mater. Interfaces 13 (2021) 61129–61138.
- [15] J. Zhang, P. Chen, W. Gao, et al., Sep. Purif. Technol. 265 (2021) 118474.
- [16] Y.L. Li, C.T. Zee, J.B. Lin, et al., J. Am. Chem. Soc. 142 (2020) 18093–18102.
- [17] J. Xie, J. Li, Y. Xie, et al., Energy 213 (2020) 118801.
- [18] J. Xu, J. Liu, P. Ling, et al., Energy 202 (2020) 117644.
- [19] K. Zhang, P. Sun, M.C.A.S. Faye, Y. Zhang, Carbon 130 (2018) 730–740.
- [20] G. Wu, C.M. Johnston, N.H. Mack, et al., J. Mater. Chem. 21 (2011) 11392.
- [21] M. Afsharpour, M. Elyasi, H. Javadian, Molecules 26 (2021) 6569.
- [22] S.R. Kelemen, M. Afeworki, M.L. Gorbaty, et al., Energy Fuels 20 (2006) 635–652.
- [23] Y. Wei, J. Miao, P.J.J. Alvarez, et al., Environ. Sci. Technol. 56 (2022) 10557–10559.
- [24] Q. Shi, S. Pu, X. Yang, et al., Chin. Chem. Lett. 33 (2022) 2129–2133.
- [25] J. Gu, P. Yin, Y. Chen, H. Zhu, R. Wang, Chin. Chem. Lett. 33 (2022) 4792–4797.
- [26] S.K. Han, T.M. Hwang, Y. Yoon, et al., Chemosphere 84 (2011) 1095–1101.
- [27] Y. Lang, S. Wu, Q. Yang, et al., Anal. Chem. 93 (2021) 9737–9743.
- [28] J.H. Wu, F. Chen, T.H. Yang, H.Q. Yu, Proc. Natl. Acad. Sci. U. S. A. 120 (2023) e2305706120.
- [29] X. Zhou, M.K. Ke, G.X. Huang, et al., Proc. Natl. Acad. Sci. U. S. A. 119 (2022) e2119492119.
- [30] M. Yang, Z. Hou, X. Zhang, et al., Environ. Sci. Technol. 56 (2022) 11635–11645.
- [31] K. Yin, R. Wu, Y. Shang, et al., Appl. Catal. B 329 (2023) 122558.
- [32] J. Miao, W. Geng, P.J.J. Alvarez, M. Long, Environ. Sci. Technol. 54 (2020) 8473–8481.
- [33] R. Luo, M. Li, C. Wang, et al., Water Res. 148 (2019) 416–424.
- [34] C. Zhu, S. Zhao, Z. Fan, et al., Adv. Funct. Mater. 30 (2020) 2003947.
- [35] P. Shao, S. Yu, X. Duan, et al., Environ. Sci. Technol. 54 (2020) 8464–8472.
- [36] K. Yin, Y. Shang, D. Chen, et al., Appl. Catal. B 338 (2023) 123029.
- [37] K. Yin, L. Peng, D. Chen, et al., Appl. Catal. B 336 (2023) 122951.
- [38] R. Zhang, M. Tahir, S. Ding, et al., ACS Appl. Energy Mater. 3 (2020) 2323–2330.
- [39] P. Wang, S. Zhan, H. Wang, et al., Appl. Catal. B 230 (2018) 210–219.
- [40] K.-Y.A. Lin, Z.Y. Zhang, Chem. Eng. J. 313 (2017) 1320–1327.
- [41] Y.L. He, C.S. He, L.D. Lai, et al., Appl. Catal. B 314 (2022) 121390.
- [42] J. Wang, Z. Chai, S. Yang, et al., J. Hazard. Mater. 459 (2023) 132094.
- [43] S. Zhang, X. Huo, S. Xu, et al., Process Saf. Environ. Prot. 168 (2022) 1219–1234.
- [44] X. Dong, B. Ren, Z. Sun, et al., Appl. Catal. B 253 (2019) 206–217.
- [45] Y. Shang, Y. Kan, X. Xu, Chin. Chem. Lett. 34 (2023) 108278.